Active Thermal Control of Distributed Parameter Systems With Application to Testing of Packaged IC Devices

Matthew Sweetland
Mem. ASME
e-mail: sweetlan@alum.mit.edu

John H. Lienhard V
Fellow ASME
e-mail: lienhard@mit.edu

W. M. Rohsenow Heat and Mass
Transfer Laboratory,
Department of Mechanical Engineering,
Massachusetts Institute of Technology,
77 Massachusetts Avenue, Room 3-162,
Cambridge, MA 02139-4307

Active control of the die-level temperature is desirable during production testing of high power microprocessors, so as to ensure accurate performance classification. Such control requires that the controlling thermal load time-lead the dissipated thermal load and that it be modulated to account for the distributed thermal capacitance and resistance of the device packaging. The analysis in this paper demonstrates fundamental limits of temperature control for typical devices under test conditions. These limits are identified for specified control power to die power ratios. The effects of test sequence design and device package design on the temperature control limits are also examined. The theory developed can be applied to any thermal control problem where a conductive medium separates the control source from the location where control is desired.
[DOI: 10.1115/1.1527908]

Keywords: Conduction, Control, Electronics, Heat Transfer, Temperature

1 Introduction

All high-performance electronic devices are subject to a 100 percent functional test prior to being shipped by the manufacturer [1]. High power microprocessor devices are also subject to a classification test to determine the effective operating speed of the device. During this classification test, the goal of control is to keep the temperature of the die at a single set temperature while the device power is varied between 0 percent to 100 percent power in a predetermined test sequence. Temperature increases over the specified test temperature decrease the signal propagation speed within the device, and an excessive temperature rise above the test temperature can result in the device being classified in the wrong category (e.g., a 1 GHz device classified and shipped as a 950 MHz device). The manufacturer normally specifies a die-level test temperature range; a typical test temperature specification is $85°C-0°C/+3°C$.

As microprocessor device powers have increased and device sizes have decreased, the power densities in packaged microprocessor devices have approached levels of 50 to 100 W/cm² [2–4]. With test sequences rapidly varying the device power at these power densities, active temperature control is essential to holding the die temperature within tolerance. Because the tests are being performed on packaged devices, thermal control cannot be applied to the die itself. Instead, control heating and cooling must be applied to some external part of the packaging. This separation of the control point from the die limits the achievable temperature control tolerances for given test sequences and device powers.

An estimate of the required control power is needed in the early design phases of temperature control systems for test equipment, so that the heating and cooling system capabilities can be specified. For this reason, an analysis of the packaged device by itself, without any consideration of the control system, is very useful in determining the required minimum heating and cooling capacities as well as in determining the effects of varying the test sequence design and package design on the thermal control limits. This paper develops such a model.

2 Mathematical Model

Semiconductor packaging encompasses a wide range of geometries, die architectures, and materials. In this paper, we consider the arrangement shown in Fig. 1. The device consists of a silicon die mounted on single or multiple interposer/interface layers. An integrated heat spreader (typically plated copper) is mounted on top of the die structure with a very thin layer of a thermal interface material or grease between the die and the heat spreader. The heat spreader area is typically much larger than the die area and provides a bonding surface for an external heat sink in the final device application. We consider situations in which the die's heat generation is essentially uniform over its area, with no large-scale variations.

Our focus is on temperature under test conditions. During testing, the packaged device is held in a test socket which is itself temperature controlled to the desired test temperature. The socket is thermally isolated from the test electronics [1,5].

Work by Viswanath et al. [6] and Sweetland [7] has shown that the thermal resistance between the die structure and the interposer layer is typically much higher than the thermal resistance between the die structure and the surface of the integrated heat spreader. For this reason, only the die and integrated heat spreader will be considered in the transient model (the interposer side of the die is considered adiabatic). If the architecture of a particular device allows non-negligible heat transfer to the interposer, the present results will provide an upper bound on the required control power and a conservative basis for design.

Several additional simplifying approximations can be made about the device under test and the operating conditions. The goal of this analysis is to determine the limits of temperature control under typical transient die power fluctuations, so only transient effects will be considered[1]. The system is initially taken to be one-dimensional. This is equivalent to neglecting the effect of *transient* lateral conduction in the integrated heat spreader; a correction factor for this approximation is given in a later section.

The interfacial resistance between the die and the integrated

---

[1]The steady state (DC) component of the temperature response of the system can be superimposed if needed.

Copyright © 2003 by ASME
Transactions of the ASME
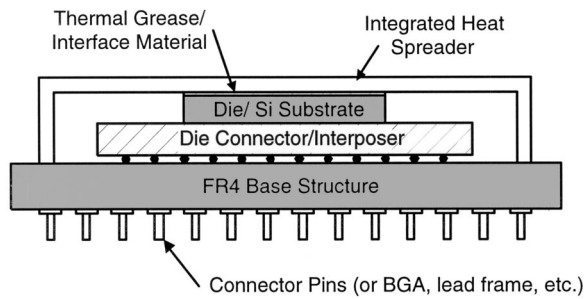
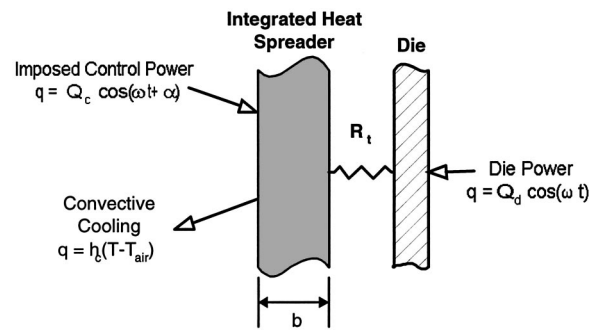**Fig. 1 Typical cross-section of a high power microprocessor device**

Fig. 2 Schematic diagram of simplified device for transient analysis. Q_c is the magnitude of the control input and α is the phase shift of the control input. Q_d is the magnitude of the die power profile.

heat spreader is assumed to be known. The heat capacitance of the interface material is neglected, since typical interface materials are thin relative to typical dies.

Temperature gradients within the die are taken to be small, effectively making the die a lumped object with uniform internal heat generation. At low frequencies, this approximation is easily justified because the thermal resistance of the interface layer is large compared to that of the die, unless the dies are very thick (>1500 μm). For higher frequencies, analysis of the unsteady conduction in the die, with heat generation confined to the face opposite the integrated heat spreader, shows that the die follows lumped response for the frequencies of importance to the die's thermal response. At sufficiently high frequencies, departures from lumped behavior occur but are associated with very small temperature variations [7]. We give a specific criterion later in the paper.

Based on these approximations, the physical system reduces to the model system shown in Fig. 2.

Various implementations of test-system temperature controls have been developed [7–9]. For the purposes of this paper, the control power is assumed to be a radiation source (a high power laser) whose power can be instantly adjusted. The front face of the integrated heat spreader is subjected to both this radiation and convective cooling. The convective conditions are constant[2], with thermal control being attained through modulation of the radiation source. This combined radiant heating/convection cooling thermal control system has the advantage that no additional thermal mass is placed in contact with the device under test, which greatly improves the transient response.

The transient part of the die test power sequence can be decomposed into component frequencies. The results will show that the control power required for a specified die temperature tolerance is a function of the test-sequence frequency. For this reason, the die power in the analysis will be assumed to be a sinusoidal signal at a fixed frequency and magnitude. Any desired test sequence can be reconstructed using sinusoids by superposition. A surface flux that provides the control power is also taken to be sinusoidal, having the same frequency but with some specified phase shift. It is important to note that the fluctuating (AC) control power is superposed on a larger, steady (DC) power so that the physical surface flux is always positive.

To start the transient analysis, only the temperature profile within the integrated heat spreader (IHS) will be considered. For mathematical convenience, that problem can be further decomposed into the two parts shown in Fig. 3. The first part is for the IHS with an adiabatic back face[3] and a front surface subject to convective cooling and the radiative control power profile (Fig. 3(a)). The second part is for the IHS with an imposed surface flux from the die on one face and convection on the other face (Fig. 3(b)). The two results are then combined using superposition. To

maintain contact with the physical variables, we do not introduce a full nondimensionalization until the solution has been constructed, at the end of this section.

2.1 IHS Temperature Response to Control Input. The steady periodic transient response to the two cases in Fig. 3 can be calculated using a complex temperature approach [10]. Consider an infinite slab with one side adiabatic as shown in Fig. 3(a). The other face is subject to convective boundary conditions, an average heat transfer coefficient h_c with an air temperature $T_{air}=0$, and a control flux $Q(t)=Q_c\cos(\omega t)$. Using complex analysis methods, it is assumed that the solution to the temperature profile in the complex plane takes the form:

$$W = X(x) \cdot \tau(t) \tag{1}$$

where $\tau(t)=e^{i\omega t}$ and $i=\sqrt{-1}$ is the imaginary number. The conduction equation in the integrated heat spreader is

$$\frac{\partial^2 W}{\partial x^2} = \frac{1}{a_t}\frac{\partial W}{\partial t} \tag{2}$$

so with an assumed solution of form Eq. (1), this can be rewritten

$$\frac{d^2 X}{dx^2} = \frac{i\omega}{a_t} \tag{3}$$

which has the general solution

$$X(x) = C_1 \exp\left(-\sqrt{\frac{i\omega}{a_t}}x\right) + C_2 \exp\left(\sqrt{\frac{i\omega}{a_t}}x\right) \tag{4}$$

The boundary conditions on Eq. (3) are as follows:

$$x=0 \quad \frac{dX}{dx}=0 \tag{5}$$

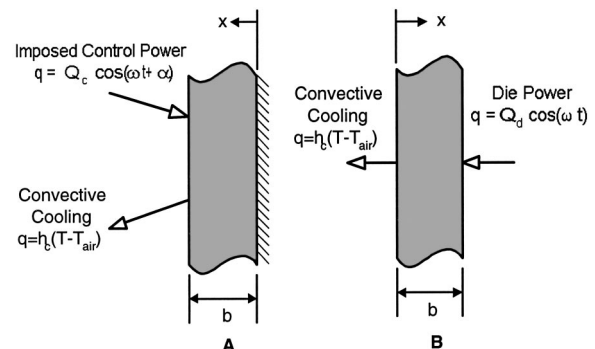**Fig. 3 Schematic drawing of decomposition for solution to transient temperature profile in integrated heat spreader**

---

[2]Fixed air temperature and constant air flow rate.
[3]Die-side face is assumed adiabatic.

$$x = b \qquad -k\frac{dX}{dx} + Q_c = h_c X \qquad (6)$$

Use of the boundary condition at $x = 0$ yields:

$$\frac{dX}{dx} = 0 = -\sqrt{\frac{i\omega}{a_t}}C_1 + \sqrt{\frac{i\omega}{a_t}}C_2 \qquad (7)$$

from which $C_1 = C_2 \equiv C$. The boundary condition at $x = b$ produces the expression:

$$h_c C[e^{-bL(i+1)} + e^{bL(i+1)}] + kC[e^{-bL(i+1)} - e^{bL(i+1)}]L(i+1)$$
$$= Q_c \qquad (8)$$

where $L \equiv \sqrt{\omega/2a_t}\,(\mathrm{m}^{-1})$. This equation must be solved for C. Expanding all exponential terms into complex sinusoids, Eq. (8) can be written as:

$$kL \cdot C(A + Bi) = Q_c e^{bL} \qquad (9)$$

where

$$A = \left\{ \frac{\mathrm{Bi_{IHS}}}{bL}\cos(bL)(e^{2bL}+1) - [\cos(bL) + \sin bL] \right.$$
$$\left. + e^{2bL}[\cos(bL) - \sin(bL)] \right\} \qquad (10)$$

$$B = \left\{ \frac{\mathrm{Bi_{IHS}}}{bL}\sin(bL)(e^{2bL}-1) - [\cos bL - \sin(bL)] \right.$$
$$\left. + e^{2bL}[\cos(bL) + \sin(bL)] \right\} \qquad (11)$$

where $\mathrm{Bi_{IHS}} = h_c b/k$ is the spreader Biot number and $bL = b\sqrt{\omega/2a_t}$ is a dimensionless frequency parameter. The Biot number is typically small compared to one. Equation (9) can now be solved for C by multiplying both sides through by the complex conjugate. Substituting the results into the original solution for X yields:

$$X = \frac{Q_c e^{bL}(A - Bi)}{kL(A^2 + B^2)}[e^{-xL(i+1)} + e^{xL(i+1)}] \qquad (12)$$

To find the solution to the temperature profile in the integrated heat spreader in the real domain, the real part of $Xe^{i\omega t}$ must be taken:

$$T(x,t) = \mathrm{Re}(Xe^{i\omega t})$$
$$= \frac{Q_c e^{bL-xL}}{kL(A^2 + B^2)}[A\cos(\omega t - xL) + B\sin(\omega t - xL)]$$
$$+ \frac{Q_c e^{bL+xL}}{kL(A^2 + B^2)}[A\cos(\omega t + xL) + B\sin(\omega t + xL)]$$
$$(13)$$

2.2 IHS Temperature Response to Die Input. An identical approach can be used to find the temperature profile of the integrated heat spreader subject to heat input from the die, but with different boundary conditions. Using the coordinate system shown in Fig. 3(b), the boundary conditions are as follows:

$$x = 0 \quad k\frac{dX}{dx} = h_c X \qquad (14)$$

$$x = b \quad Q_d = k\frac{dX}{dx} \qquad (15)$$

With Eq. (4) for X, the boundary condition at $x = 0$ yields:

$$k\sqrt{\frac{i\omega}{a_t}}(C_2 - C_1) = h_c(C_1 + C_2) \qquad (16)$$

This equation can be solved to express the new C_1 in terms of the new C_2:

$$C_1 = C_2 \frac{2(kL)^2 - h_c^2 + (2h_c kL)i}{h_c^2 + 2kh_c L + 2(kL)^2} \qquad (17)$$

in which $L = \sqrt{\omega/2a_t}$ as before. Defining

$$D = h_c^2 + 2kh_c L + 2(kL)^2, \quad E = 2(kL)^2 - h_c^2, \quad F = 2h_c kL \qquad (18)$$

Eq. (17) can be written

$$C_1 = C_2 \frac{(E + Fi)}{D} \qquad (19)$$

and the solution for X becomes

$$X = C_2\left[\frac{E+Fi}{D}\exp\left(-\sqrt{\frac{i\omega}{a_t}}x\right) + \exp\left(\sqrt{\frac{i\omega}{a_t}}x\right) \right] \qquad (20)$$

Substitution of this expression into the boundary condition at $x = b$ produces

$$Q_d = C_2 kL\left[(i+1)e^{bL}e^{bLi} - \frac{e^{-bL}}{D}(E+Fi)(i+1)e^{-bLi} \right] \qquad (21)$$

which may be rearranged to

$$\frac{Q_d}{C_2 kL} = e^{bL}[\cos(bL) - \sin(bL)] - \frac{e^{-bL}}{D}[G\cos(bL) + N\sin(bL)]$$
$$+ e^{bL}i[\sin(bL) + \cos(bL)]$$
$$- \frac{e^{-bL}}{D}i[-G\sin(bL) + N\cos(bL)] \qquad (22)$$

where

$$G = E - F \quad \text{and} \quad N = E + F. \qquad (23)$$

With the following additional definitions

$$P = e^{bL}[\cos(bL) - \sin(bL)] - \frac{e^{-bL}}{D}[G\cos(bL) + N\sin(bL)] \qquad (24)$$

$$R = e^{bL}[\sin(bL) + \cos(bL)] + \frac{e^{-bL}}{D}[G\sin(bL) - N\cos(bL)] \qquad (25)$$

the solution for the constant C_2 may be written

$$C_2 = \frac{Q_d(P - Ri)}{kL(P^2 + R^2)} \qquad (26)$$

The function X is therefore

$$X = \frac{Q_d(P-Ri)}{kL(P^2+R^2)}\left[\frac{(E+Fi)}{D}e^{-xL(i+1)} + e^{xL(i+1)} \right] \qquad (27)$$

The solution for the temperature in the heat spreader is again found by solving for the real part of $Xe^{i\omega t}$. Setting

$$U = \frac{P \cdot E + R \cdot F}{D} \quad \text{and} \quad V = \frac{P \cdot F - E \cdot R}{D} \qquad (28)$$

the final expression for the temperature of the heat spreader is

$$T(x,t) = \mathrm{Re}(Xe^{i\omega t}) = \frac{Q_d e^{-xL}}{kL(P^2+R^2)}[U\cos(\omega t - xL)$$
$$- V\sin(\omega t - xL)] + \frac{Q_d e^{xL}}{kL(P^2+R^2)}[P\cos(\omega t + xL)$$
$$+ R\sin(\omega t + xL)] \qquad (29)$$

We note that P, R, U, and V depend on bL and $\mathrm{Bi_{IHS}}$ only.

2.3 IHS Combined Temperature Response. The temperature response of the integrated heat spreader to concurrent control and die heat inputs is found using superposition. In particular, we seek the temperature on the face of the IHS that contacts the die. That temperature is obtained by adding the solution for the control input at $x=0$, Eq. (13), to the solution for the die input at $x=b$, Eq. (29), recalling that the x coordinates differ for the two solutions. A phase shift, α, must be added to the solution for the control input in order to calculate the required amplitude and phase lag of the control heat input for a desired IHS temperature; this simply means substituting $(\omega t + \alpha)$ for (ωt) in Eq. (13). After some algebra, the final temperature response on the die-side face of the IHS is:

$$T_{\text{IHS}} = \frac{2Q_c e^{bL}}{kL(A^2+B^2)} \{[A \cos\alpha + B \sin\alpha]\cos(\omega t) + [B \cos\alpha$$

$$- A \sin\alpha]\sin(\omega t)\} + \frac{Q_d e^{-bL}}{kL(P^2+R^2)} \{[U \cos(bL)$$

$$+ V \sin(bL)]\cos(\omega t) + [U \sin(bL) - V \cos(bL)]\sin(\omega t)\}$$

$$+ \frac{Q_d e^{bL}}{kL(P^2+R^2)} \{[P \cos(bL) + R \sin(bL)]\cos(\omega t)$$

$$- [P \sin(bL) - R \cos(bL)]\sin(\omega t)\}. \tag{30}$$

From this result, for any specified power dissipation amplitude on the die Q_d and any desired IHS die-side temperature response T_{IHS}, the control power amplitude Q_c and phase shift α required can be calculated. For example, to obtain a constant temperature at the die contact point on the integrated heat spreader ($T_{\text{IHS}}=0$, say), the magnitude and phase shift of the control signal are found by solving the equation:

$$\{PS_2 \cdot [A \cos\alpha + B \sin\alpha] \cdot Q_c + PS_1 \cdot e^{-bL}[U \cos(bL)$$

$$+ V \sin(bL)] + PS_1 \cdot e^{bL}[P \cos(bL) + R \sin(bL)]\}\cos(\omega t)$$

$$+ \{PS_2 \cdot [B \cos\alpha - A \sin\alpha] \cdot Q_c + PS_1 \cdot e^{-bL}[U \sin(bL)$$

$$- V \cos(bL)] + PS_1 \cdot e^{bL}[R \cos(bL) - P \sin(bL)]\}\sin(\omega t)$$

$$= 0 \tag{31}$$

with

$$PS_1 = \frac{Q_d}{kL(P^2+R^2)} \quad PS_2 = \frac{2e^{bL}}{kL(A^2+B^2)} \tag{32}$$

Since Eq. (31) must hold for any time t, the solution for Q_c and α may be obtained by requiring that coefficients of the sine and cosine terms of Eq. (31) vanish separately. This yields two equations which define Q_c as a function of α:

$$\left\{\frac{2e^{bL}[A \cos\alpha + B \sin\alpha]}{A^2+B^2}\right\} \cdot \frac{Q_c}{Q_d} = -\left\{\frac{e^{-bL}[U \cos(bL) + V \sin(bL)] + e^{bL}[P \cos(bL) + R \sin(bL)]}{P^2+R^2}\right\} \tag{33}$$

$$\left\{\frac{2e^{bL}[B \cos\alpha - A \sin\alpha]}{A^2+B^2}\right\} \cdot \frac{Q_c}{Q_d} = -\left\{\frac{e^{-bL}[U \sin(bL) - V \cos(bL)] + e^{bL}[R \cos(bL) - P \sin(bL)]}{P^2+R^2}\right\} \tag{34}$$

The solution to these simultaneous equations is the intersection point of a graph of the sine and cosine for Q_c as a function of α; a dimensional example is shown in Fig. 4. For a 10 Hz die power profile with a magnitude of $Q_d = 10 \text{ W/cm}^2$, the solution for the control power profile to obtain a constant temperature on the back face of the IHS is a 10 Hz control profile with a phase shift of $\alpha = 226.1$ deg and an amplitude $Q_c = 12.5 \text{ W/cm}^2$.

In nondimensional terms, factors in braces in these equations depend only upon the dimensionless frequency parameter, bL, and the Biot number of the IHS, Bi_{IHS}. Thus, the dimensionless control power required, Q_c/Q_d, is a function of (bL) and Bi_{IHS}.

The solution for Q_c under given conditions can be used to generate the temperature profile in the IHS under steady periodic conditions. Figure 5 presents the temperature response in the IHS if only the die power profile is imposed, continuing the example begun in Fig. 4. As can be seen, the temperature of the IHS at the die interface fluctuates at 10 Hz, as does the convection side of the IHS. The maximum and minimum temperatures through the IHS are plotted in the bottom frame of Fig. 5. A phase shift occurs between the temperatures on the two faces, and the amplitude on the die side is slightly larger than the convection side.

If a control profile of magnitude $Q_c = 12.5 \text{ W/cm}^2$ and phase lag of $\alpha = 226.1$ deg is applied to the convection side of the IHS, the resulting IHS temperature profile is shown in Fig. 6. As can be seen, the temperature variation at the die side contact face of the IHS can be reduced to zero by application of the control power profile.

2.4 Temperature Response of Die. The die normally has small thermal resistance and can be treated as isothermal for the frequencies of interest. Its temperature response is described by

$$m \cdot c_p \frac{dT_{\text{die}}}{dt} = Q_d \cdot \cos(\omega t) - \frac{T - T_{BF}}{R_t} \tag{35}$$

where m is the mass of die per unit area and T_{BF} is the die-side surface temperature of the integrated heat spreader. This equation neglects the heat capacity of the thermal interface material between the die and the IHS. For ideal temperature control, where
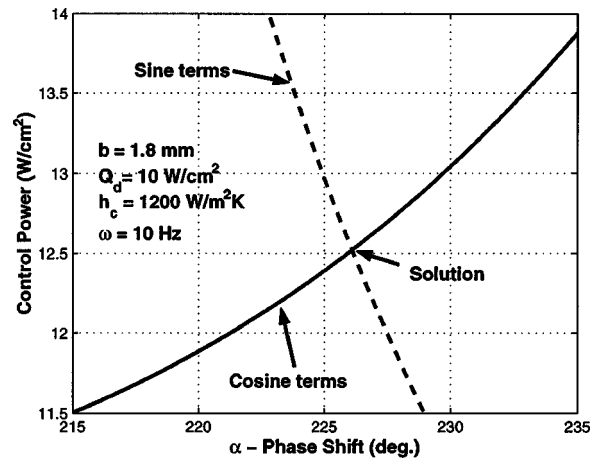

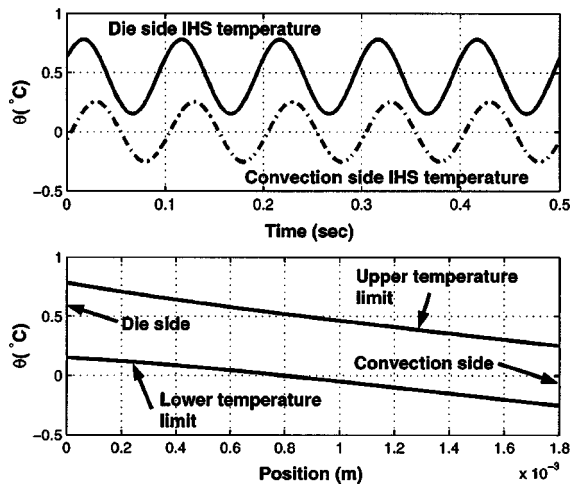**Fig. 4 Solution for phase shift and magnitude of control power profile**

Fig. 5 Temperature response of IHS to a 10 Hz die power profile with $Q_d = 10$ W/cm². For this system, $h_c = 1200$ W/m² and the IHS is 1.8 mm thick.
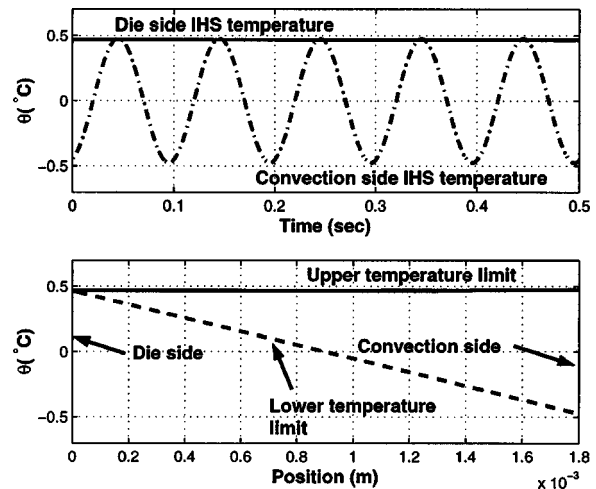
Fig. 6 Temperature response of IHS to a 10 Hz die power profile with $Q_d = 10$ W/cm² and a control power profile imposed on the front face

there is no change in die temperature, and taking the desired die temperature be zero[4], the equation for the IHS back face temperature becomes:

$$T_{BF} = -Q_d \cdot R_t \cos(\omega t) = Q_d \cdot R_t \cos(\omega t + \pi) \qquad (36)$$

The second expression clearly shows that for ideal temperature control, the desired IHS back face temperature is 180 deg out of phase with the die power profile with a magnitude that depends on Q_d and the thermal interface resistance R_t. Returning to the example in Fig. 5, to obtain constant die temperature, the desired back-face temperature must be obtained by appropriate scaling of the control profile. To find this control profile, Eq. (31) must be solved, but instead of zero on the righthand side of the equation, the term $(-Q_d \cdot R_t \cos(\omega t))$ must be used. Again separating the sine and cosine terms, the solution for the power profile can be found.

The desired control profile phase shift to obtain a constant die temperature with a die power density of $Q_d = 10$ W/cm² is $\alpha = 283.42$ deg with a magnitude of $Q_c = 173.0$ W/cm². The phase shift calculated here is a phase lag between the die input and the control input, which may alternatively be regarded as a phase *lead* of 76.58 deg with the control power profile leading the die power profile. This is important when the analysis turns to control limits for a die power profile.

From these results, the temperature profile in the IHS can again be calculated, as in Fig. 7, which also shows the die power profile and the target temperature, T_{BF}. Although the target temperature can be again maintained, a significantly higher control power is required relative to the previous case (for which T_{BF} was held constant). The ratio of control power to die power has risen from 1.25 to 17.30. This is because the entire mass of the IHS must now be driven over a much wider temperature range. Similar calculations can be performed over the full range of frequencies and powers.

2.5 Control Profile Calculation With Specified Die Temperature Tolerance. The two previous analyses identify the control profile for the cases where the die temperature is constant (ideal control) or where the temperature of the back face of the IHS is held constant. To reach actual practice, we must go a step further and allow the die temperature to fluctuate within specified

tolerance limits for a given die power profile (non-ideal control). We now adapt the previous analyses to obtain the control power profile for a varying die temperature.

In the light of Eqs. (35) and (36), we may assume that for non-ideal control, the back face temperature of the IHS has the form

$$T_{BF} = M \cdot R_t \cdot Q_d \cos(\omega t + \beta) \qquad (37)$$

where the scaling factor M takes on a value between 0 and 1. Upon substituting Eq. (37) into Eq. (35) and integrating, we obtain

$$T_{\text{die}} = \frac{Q_d}{mc_p(\lambda^2 + \omega^2)} \{ (1 + M \cos \beta)[\lambda \cos(\omega t) + \omega \sin(\omega t)]$$
$$- \sin \beta[\lambda \sin(\omega t) - \omega \cos(\omega t)] \} \qquad (38)$$
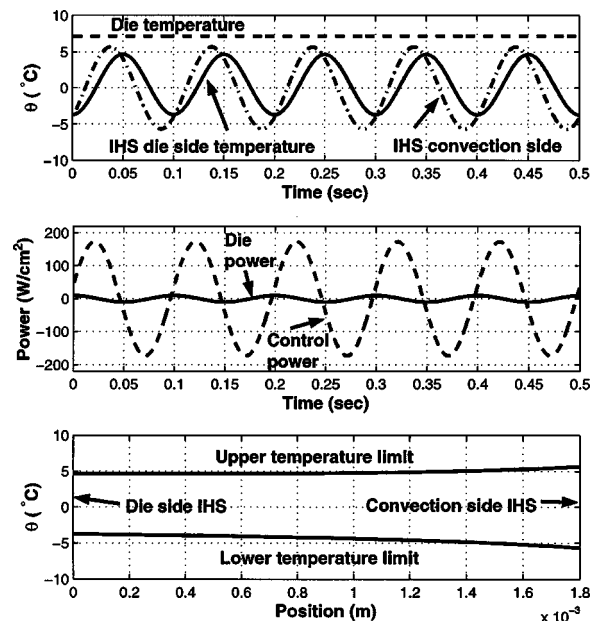
Fig. 7 IHS temperature profile for ideal control of die temperatures

where $\lambda \equiv 1/mc_p R_t$ ($1/\lambda$ is the lumped-capacity time constant associated with Eq. 35). Of interest here is the magnitude of the fluctuation of T_{die}. By setting this magnitude equal to the allowed tolerance ΔT of the die temperature, a relationship between the scaling factor M and the phase shift β is obtained:

$$M = -\cos\beta \pm \sqrt{\cos^2\beta - 1 + (mc_p \Delta T/2Q_d)^2(\omega^2 + \lambda^2)} \quad (39)$$

The goal is to minimize M for a given die power profile, since a smaller value of M leads to a smaller required control power. Equation (39) can be differentiated with respect to β

$$\frac{dM}{d\beta} = \sin\beta \mp \frac{\cos\beta\sin\beta}{\sqrt{\cos^2\beta - 1 + (mc_p \Delta T/2Q_d)^2(\omega^2 + \lambda^2)}} = 0 \quad (40)$$

This equation has two roots: $\beta = 0$ and $\beta = \pi$. For the case $\Delta T = 0$, the solution must be $M = 1$, not $M = -1$, so the correct root is $\beta = \pi$. Hence,

$$M = 1 - \frac{mc_p \Delta T}{2Q_d}\sqrt{\lambda^2 + \omega^2} = 1 - \frac{\Delta T}{2Q_d R_t}\sqrt{1 + \omega^2/\lambda^2} \quad (41)$$

which determines the magnitude of the fluctuation of T_{BF}.

One more issue must be addressed in order to find the required control power profile. The flux from the die into the heat spreader is no longer equal to the die power profile because some of the die power is taken up by the heat capacity of the die and stored in the form of a steady periodic die temperature change. From the preceding analysis, the die temperature profile is

$$T_{\text{die}} = \frac{Q_d(1-M)}{mc_p(\lambda^2 + \omega^2)}[\lambda\cos(\omega t) + \omega\sin(\omega t)] \quad (42)$$

The heat flux from the die into the heat spreader, Q_{ds}, may be calculated from Eqs. (37) and (42)

$$Q_{ds} = \frac{T_{\text{die}} - T_{BF}}{R_t} = \left(\frac{Q_d \lambda(1-M)}{mc_p R_t(\lambda^2 + \omega^2)} + MQ_d\right)\cos(\omega t)$$
$$+ \frac{Q_d \omega(1-M)}{mc_p R_t(\lambda^2 + \omega^2)}\sin(\omega t) \quad (43)$$

$$Q_{ds} = Q_d\sqrt{\frac{\lambda^2 + M^2\omega^2}{\lambda^2 + \omega^2}}\cdot\cos(\omega t + \gamma) \equiv Q_{da}\cos(\omega t + \gamma)$$

where γ is given by

$$\gamma = \tan^{-1}\left[\frac{\omega\lambda(M-1)}{\lambda^2 + M\omega^2}\right] \quad (44)$$

and the amplitude Q_{da} is defined as shown. The heat flux from the die into the integrated heat spreader is reduced in magnitude and shifted by a phase lag γ.

These revised solutions for the magnitude and phase shift of the flux and temperature at the die-side of the IHS can now be used in Eq. (30), by setting T_{IHS} in Eq. (30) to T_{BF} from Eq. (37) and setting Q_d in Eq. (30) to Q_{da} from Eq. (43). Upon separating the sine and cosine terms, there obtains:

$$\{PS_2 \cdot [A\cos\alpha + B\sin\alpha]\cdot Q_c + PS_3 e^{-bL}\cdot[U\cos(bL - \gamma)$$
$$+ V\sin(bL - \gamma)] + PS_3 e^{bL}\cdot[P\cos(bL + \gamma) + R\sin(bL$$
$$+ \gamma)]\}\cos(\omega t) + \{PS_2\cdot[B\cos\alpha - A\sin\alpha]\cdot Q_c + PS_3 e^{-bL}$$
$$\cdot[U\sin(bL - \gamma) - V\cos(bL - \gamma)] - PS_3 e^{bL}[P\sin(bL + \gamma)$$
$$- R\cos(bL + \gamma)]\}\sin(\omega t) = -R_t M\cdot Q_d\cos(\omega t) \quad (45)$$

where PS_3 is defined as

$$PS_3 = \frac{Q_{da}}{kL(P^2 + R^2)} \quad (46)$$

Equation (45) is solved in the same way as Eq. (31), by requiring that the sine and cosine terms vanish simultaneously:

$$\left\{\frac{2e^{bL}[A\cos\alpha + B\sin\alpha]}{A^2 + B^2}\right\}\cdot\frac{Q_c}{Q_d}\cdot\frac{Q_d}{Q_{da}} = -M\cdot\frac{bL}{\text{Bi}_{ds}}\cdot\frac{Q_d}{Q_{da}}$$
$$-\left\{\frac{e^{-bL}[U\cos(bL - \gamma) + V\sin(bL - \gamma)] + e^{bL}[P\cos(bL + \gamma) + R\sin(bL + \gamma)]}{P^2 + R^2}\right\} \quad (47)$$

$$\left\{\frac{2e^{bL}[B\cos\alpha - A\sin\alpha]}{A^2 + B^2}\right\}\cdot\frac{Q_c}{Q_d}\cdot\frac{Q_d}{Q_{da}} = -\left\{\frac{e^{-bL}[U\sin(bL - \gamma) - V\cos(bL - \gamma)] + e^{bL}[R\cos(bL + \gamma) - P\sin(bL + \gamma)]}{P^2 + R^2}\right\} \quad (48)$$

where $\text{Bi}_{ds} \equiv b/(kR_t)$ is a Biot number for the die side of the IHS.

As previously noted, the coefficients (A,B,P,R,U,V) depend upon the dimensionless parameters bL and Bi_{IHS}. The factors Q_d/Q_{da}, M, and γ depend on the additional dimensionless groups $Q_d R_t/\Delta T$ and ω/λ. The latter parameter can be rewritten as

$$\frac{\omega}{\lambda} = (bL)^2\left(\frac{2a_t mc_p R_t}{b^2}\right) \equiv (bL)^2 S \quad (49)$$

in which the dimensionless parameter S is the ratio of the lumped timescale of the die to the diffusion timescale of the IHS. We find, therefore, that the dimensionless control power Q_c/Q_d and phase shift α each depend upon five dimensionless variables: bL, Bi_{IHS}, Bi_{ds}, $Q_d R_t/\Delta T$, and S. Among these, only bL is dependent upon the signal frequencies used during testing. Thus, adjust-

ing the range of bL selected in a test sequence most easily adjusts the required control power, since no redesign of the device or its packaging is required.

As a dimensional example, when $Q_d = 10$ W/cm^2 and $\omega = 10$ Hz with $\Delta T = 4$ K, the required control power profile has a phase shift $\alpha = 277.2$ deg and a control magnitude of $Q_c = 63.05$ W/cm^2. This performance is much better than for ideal temperature control where the control magnitude was found to be 173.0 W/cm^2. The resulting temperature profiles for the die and the back face of the IHS are shown in Fig. 8.

2.6 Model Confirmation. In order to provide an independent confirmation of the mathematical solution, an implicit finite difference model [11] of the die/heat spreader system was constructed. The details of this solution method will be outlined in a
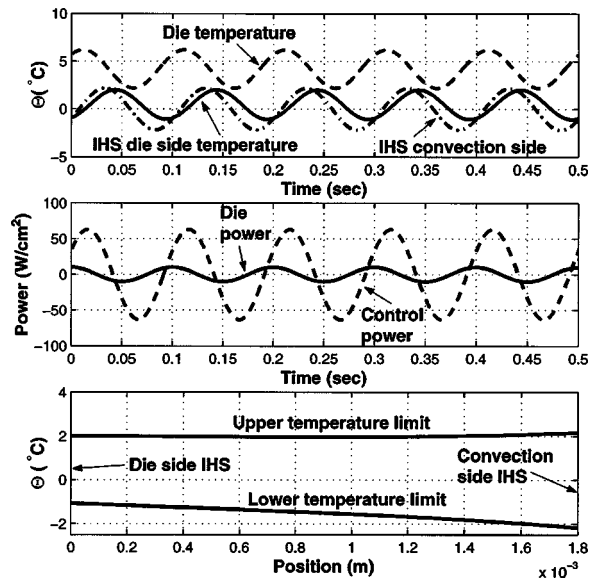
Fig. 8 Temperature profile for die and back-face of IHS for ω=10 Hz, Q_d=10 W/cm² and a tolerance ΔT=4 K
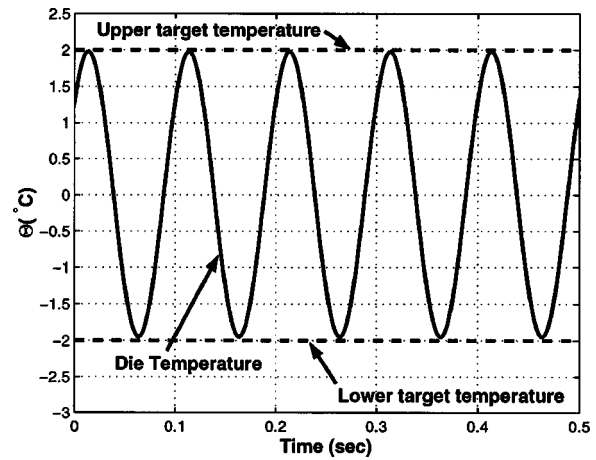

Fig. 9 Calculated die temperature using finite difference model to confirm analytic solution for control input. Target ΔT is 4 K with h_c=1200 W/m²K, R_t=0.42 cm²K/W, b=1.8 mm, and Q_d=10 W/cm².

later section, where the same method is used to estimate lateral conduction effects in the IHS. This approach is not very convenient for determining for the required control input magnitude and phase shift, but it is very useful for checking the analysis.

Figure 9 shows the die temperature as calculated from the finite difference model for a 10 Hz die power with Q_d= 10 W/cm². The control input has Q_c=63.05 W/cm² and α=277.2 deg, as predicted by the analysis for a tolerance of ΔT=4 K. As can be seen, the finite difference model confirms that the predicted control input does control the die temperature to the desired level.

3 Control of Non-Sinusoidal Die Power Profile

Any periodic or finite length die power profile can be decomposed into a Fourier series of sinusoidal terms, each of which satisfies the analyses of the previous sections. The results can be superposed to find the temperature response for the actual die power profile. In any such decomposition, a steady (DC) component must also be added so that the power inputs are non-negative.

For example, a square-wave die power profile can be written as [12]

$$Q_{sq}(t)= \frac{4Q}{\pi} \sum_{n=1,3,5\ldots} \frac{1}{n} \sin\left(\frac{2n\pi t}{\tau}\right) \qquad (50)$$

where Q is the amplitude of the square wave[5] and τ is its period. Each of these components can now be analyzed using the method developed previously in order to determine the required control input at each specific frequency. In order to do this, the temperature tolerance at each frequency must be specified in such a way that the total temperature tolerance of the die is maintained. For any specified total temperature tolerance, many solutions are possible; however, we desire the solution that minimizes control power required.

For example, suppose that desired total die temperature tolerance is ΔT=4 K on a 5 Hz square-wave signal having Q_d = 10 W/cm² and h=1200 W/m²K. The control input may be broken down into an initial allowance of ΔT=1 K for the first frequency component of the decomposition, 1 K for the second component, 1 K for the third, and 1 K for the fourth. For this initial guess, it can quickly be shown that the third and fourth components produce die fluctuations much lower than the target values

of ΔT=1 K, so that no control power is actually needed at these two frequencies. The required rms power for the two remaining frequencies is 57.2 W/cm². If the analysis is redone with ΔT =2 K on the first and second components only, the required rms control power is 43.3 W/cm², and with ΔT=2.5 K on the first frequency, 1.2 K on the second frequency, and 0.3 on the third frequency, the required rms control power is 32.0 W/cm². Multiple iterations are generally required to find the optimal solution; it is beyond our present scope to develop a systematic algorithm for these iterations. For the current example, an optimized result (Fig. 10) puts ΔT=2.3 K on the first component (5 Hz), ΔT =1.0 K on the third (15 Hz), and ΔT=0.7 K on the fifth (25 Hz), requiring 29.0 W/cm² rms control power.

A similar analysis can be performed for power profiles of any shape. A triangular wave can be expressed as the Fourier series [12]

$$Q_{tr}(t)= \frac{8Q}{\pi^2} \sum_{n=1,3,5\ldots} \frac{(-1)^{(n-1)/2}}{n^2} \sin\left(\frac{2n\pi t}{\tau}\right) \qquad (51)$$
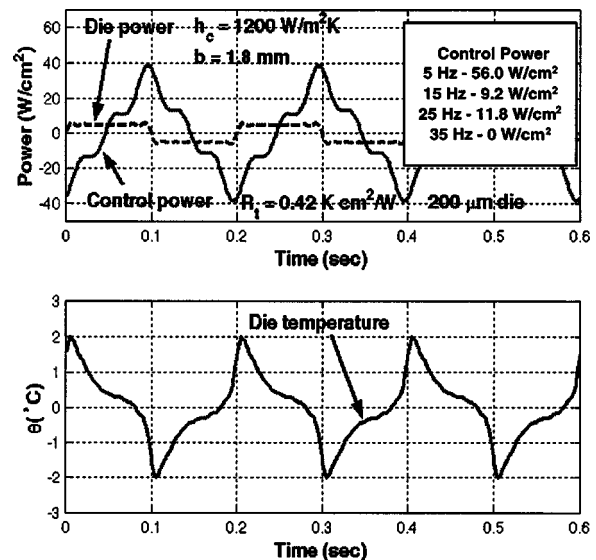

Fig. 10 Die and control powers and die temperature change, θ, for square-wave die power profile
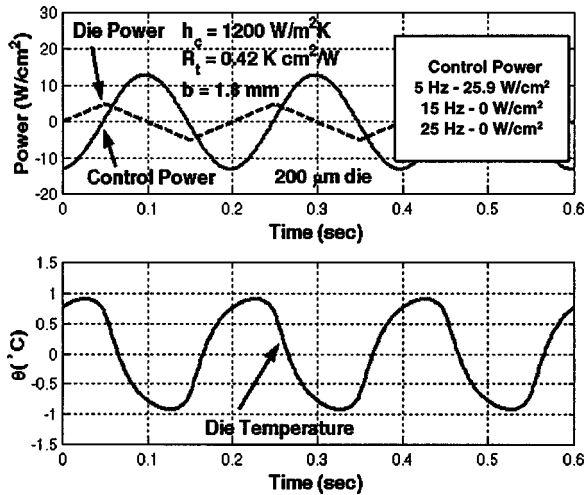
---

[5]Half the peak to peak amplitude.

Fig. 11 Die and control powers and die temperature change, θ, for triangle-wave die power profile

Fig. 12 Control power limits for specified die power amplitude, Q_d, and die temperature tolerance, ΔT, as a function of nondimensional die power frequency, $(bL)^2$

Using this decomposition, the control input for a desired level of die temperature control can be calculated. The solution in this case is fairly simple as only the first frequency term in the series requires control, so the entire ΔT tolerance can be applied to the first term. The results for a triangular wave decomposition are shown in Fig. 11.

Note the big difference in control power required between the triangular wave and square wave die power profiles. The square wave needs almost an 8:1 control to die power ratio to hold the die temperature within 4 K, whereas the triangular wave requires only a 2.4:1 ratio to hold a tighter tolerance of 2 K. Sudden changes in die power (as seen in a square wave) require much higher control power to hold a given temperature tolerance than do more slowly varying power profiles (such as the triangle wave).

4 Limits to Control for a Given Die Power Profile

A knowledge of the required control power profile for a given temperature tolerance in the die can be used to define the control limits for any given system. Specifically, for a given die power frequency and amplitude, if the control power is limited to some finite value then the die temperature can be controlled only to some minimum tolerance. Tighter temperature control is *not* possible for that level of control power.

Over a range of die power frequencies, the control power ratio, Q_c/Q_d, can be found for a given die temperature tolerance, scaled into the die power as $Q_d R_t/\Delta T$. By evaluating the control power ratio over a range of frequencies, we may define a control limit plot for a specified set of die conditions. Figure 12 shows such control limits over a range of dimensionless frequency, $(bL)^2$. In this graph, $Bi_{IHS} = 0.0055$, $Bi_{ds} = 0.11$, and $S = 0.76$, corresponding to a 200 μm thick die, a 1.8 mm thick copper IHS, $R_t = 0.42\,\mathrm{cm^2K/W}$, and convective cooling through $h_c = 1200\,\mathrm{W/m^2K}$. (Those values are typical of test conditions currently being developed [7].)

An expanded view of the same data is shown in Fig. 13. These figures illustrate the limits of control. There are three regions in Fig. 13, each representing a different region of operation. The area to the left of each curve represents a region where the temperature of the die can be controlled by applying the control power associated with that curve. The region to the right of the lines represents a region where the die power frequency is so high that no control is required to maintain the temperature tolerance limits on the die. The region contained under the curve is a regime where the specified control cannot be attained with the specified control power/die power ratio.
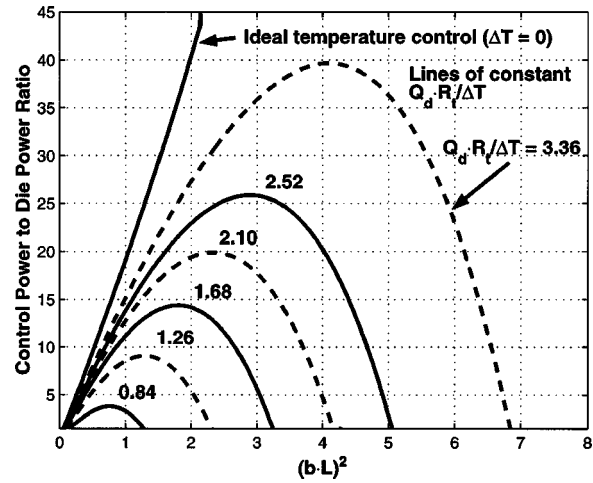
Figure 12 shows that any desired die flux to temperature tolerance ratio can be obtained with sufficient control power, so no theoretical limit to temperature control exists. On a practical level, however, power ratios over 3 or 4 quickly become impractical due to cooling requirements of the effective steady state heat load—the sum of the DC components of die power and control power. (Recall that this analysis was for the periodic components of the power profiles; in practice, both profiles also have steady components, since the instantaneous powers are never negative.)

These results lead to some very important points. The position of the lefthand sides of the curves are defined by the physical configuration of the heat spreader (thickness, conductivity, etc.), whereas the righthand sides are defined by the mass of the die, frequency of the die power profile, and thermal interface resistance between the die and the IHS. If the design of the IC device cannot be altered for thermal purposes, as is usually the case, a desired level of temperature control may instead be obtained by designing the circuit test sequence, for example, so that the die power profile always lies to the right side of the figure.

We may also evaluate the effect of design changes to the integrated heat spreader and thermal interface between the die and IHS. Changing the thermal resistance between the die and the IHS
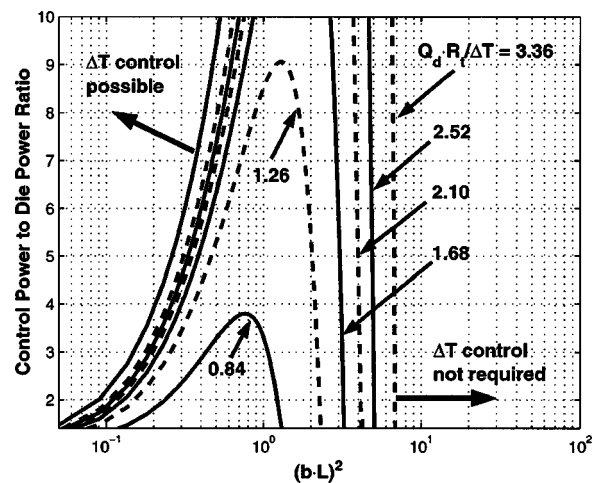

Fig. 13 Control power limits for specified die power amplitude, Q_d, and die temperature tolerance, ΔT, as a function of nondimensional die power frequency, $(bL)^2$
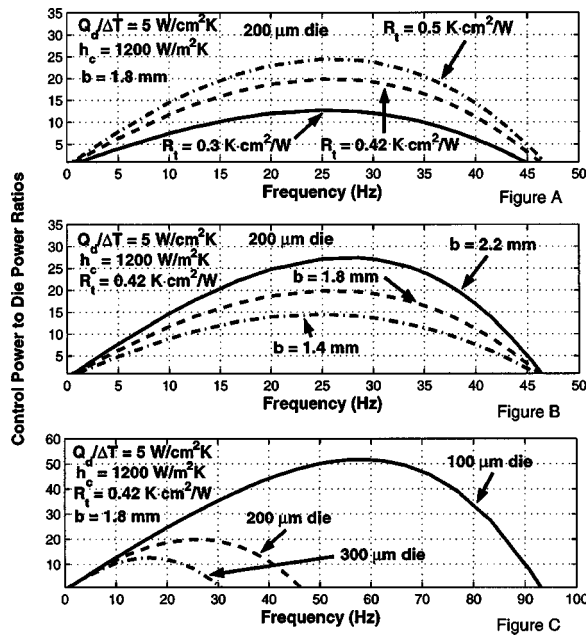
Fig. 14 Effect on control power limits of: (*a*) interfacial thermal resistance; (*b*) IHS thickness; and (*c*) die thickness.
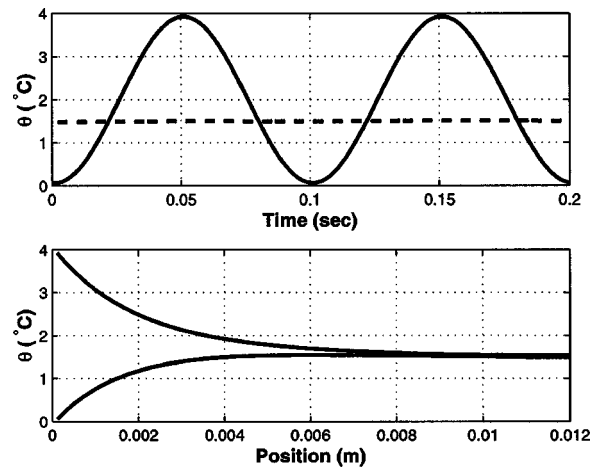

Fig. 15 Transient fin temperature profile for 10 Hz example. Top: temperature variation at base and tip of fin. Bottom: maximum/minimum temperature defect along the length of the fin.

can have a profound effect on the control limits at higher power ratios. This is seen in Fig. 14(*a*) for $Q_d/\Delta T = 5$ W/cm²K. The effects of changing the thickness of the integrated heat spreader and the die are shown in Fig. 14(*b*) and Fig. 14(*c*), respectively. Changing the thickness of the die (and therefore its mass) has the largest impact on the control limits of the device. The increasing the thickness of the IHS also raised the power required for a given level of control. The effect of changing the convective transfer coefficient h_c is negligible, with no change observed when h_c varies from 500 W/m²K to 2000 W/m²K.[6]

4.1 Limitations of the Isothermal Die Approximation. The techniques used to analyze the IHS can also be applied to heat conduction in the die as a check on the lumped capacitance model for the die. The results of such analysis show that a die of thickness δ can be treated as isothermal for frequencies low enough that $\delta^2\omega/(2a_t) < 0.3$ to 0.4. For the baseline die considered here, that corresponds to frequencies of 200 to 300 Hz and $(bL)^2 < 30$ to 40. It must also be noted that the temperature variations associated with the higher frequencies tend to be quite small.

5 Lateral Conduction Effects in IHS

The function of the heat spreader is to act as a fin, conducting heat laterally away from the die. For the steady components of die power, the IHS will indeed function as a fin. For higher frequency components, however, the fin effect will be limited to a frequency-dependent thermal penetration length in the IHS near the die. Only the lower frequency components will have a sufficient penetration depth to influence the control response. In this section, we examine the effect of frequency-dependent lateral conduction on the control requirements.

The Biot number, $\mathrm{Bi_{IHS}}$, for a typical heat spreader is very small, even at the highest h_c values considered here (e.g., $\mathrm{Bi_{IHS}} = 0.009$ for $h_c = 2000$ W/m²K and $b = 1.8$ mm). Thus, the thermal response of the parts of the spreader beyond the die can be modelled using the unsteady fin equation

---

[6]These values are typical of the air-jet array cooling we have implemented and measured in such systems. Small nozzle diameters, modest air pressures, and close nozzle-to-nozzle spacings are required.

$$\frac{\partial^2 \Theta}{\partial x^2} + \frac{1}{A(x)}\frac{dA}{dx}\frac{\partial \Theta}{\partial x} - \frac{hP}{kA(x)}\Theta = \frac{1}{a_t}\frac{\partial \Theta}{\partial t} \qquad (52)$$

where $\Theta = T - T_{\mathrm{air}}$, P is the perimeter subject to convection, $A(x)$ is the cross-sectional area, and a_t is the thermal diffusivity.

A square heat spreader with a square die can be broken into four identical quadrants, by symmetry. The cross-sectional area of the heat spreader can now be expressed as $A(x) = A_0 + 2\alpha \cdot b \cdot x$, where A_0 is the area of the fin along the line of contact with the die and $\alpha = 0.5$.

Equation (52) has been studied extensively, and analytical solutions have been reviewed by Aziz and Kraus [13]. In the present case, with variable cross-sectional area and time dependent boundary conditions, the equation will be solved using discrete methods. The two items of principal interest are the heat flux and the thermal penetration depth that result from a change in base temperature, with the latter corresponding to the temperature of the IHS directly over the die structure.

The base temperature is never uniform across the thickness of the heat spreader because the powers are time dependent (as shown in previous sections). Nevertheless, this temperature varies over a well specified range, and a bounding value can be used to examine the worst case losses into the fin-like parts of the IHS away from the die. The magnitude of the temperature variation in the IHS over the die can be taken from the previously determined IHS temperature profiles, such as Fig. 8.

Using an implicit finite difference method [11], the fin may be divided into the N sections shown in the inset in Fig. 16. The temperature of a fin section subject to time varying boundary conditions can be written as

$$\mathbf{A} \cdot \mathbf{T}^{i+1} = \mathbf{T}^i + \mathbf{F} \qquad (53)$$

where $[\mathbf{T}^i]$ and $[\mathbf{T}^{i+1}]$ are arrays of the fin temperature at time step i and $i+1$ respectively. The details of the forcing function $[\mathbf{F}]$ and characteristic matrix $[\mathbf{A}]$ are standard, and will not be repeated here (see [7] for details). The temperature at time step $i + 1$ is found by matrix inversion.

We used this approach to determine the temperature profile in the fin as a function of time subject to changing base temperature T_b^i. The fin was broken into 100 segments and the time step Δt was decreased by factors of two until successive changes in the time step produced results that varied by less than 0.01°C at all times.

The heat lost by conduction into the IHS away from the die is found by integrating the flux into the base area, A_0, over a full
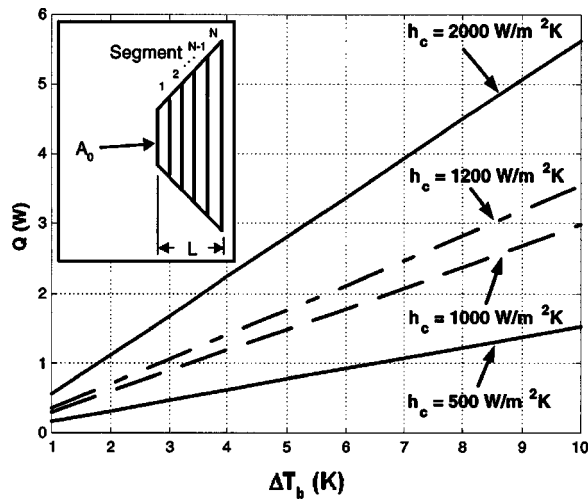
Fig. 16 Lateral conduction into IHS for various h_c: Q=cyclic lateral loss into IHS; ΔT_b=temperature fluctuation amplitude of IHS at die edge. Insert shows discretization of IHS for numerical solution.

period of the harmonic power variation. This heat may be viewed as lost control energy. For example, consider a 1 cm² die that has a 1.8 mm thick heat spreader measuring 3.4 cm by 3.4 cm. The temperature profile in the part of the IHS not above the die is shown in Fig. 15 for a 10 Hz base temperature variation having a peak-to-peak magnitude of 4 K with $h_c = 1200$ W/m²K. The cyclic heat loss is 0.36 W per fin segment, or 1.44 W for the entire heat spreader. Similar calculations have been done for a range of frequencies and for various h_c (Fig. 16).

The results of such analyses can be used in one of two ways to correct the control response for the lateral conduction losses. One approach is simply to add the control losses to the total control power. The second approach is to provide a control heat flux to an area of the heat spreader larger than the die, so as to minimize time-dependent lateral heat loss from the die (in the case of laser heating of the IHS, this amounts to over-illumination of the IHS). The second option is only really possible for higher frequency signals, because at lower frequencies the penetration depth is of the same order of magnitude as the width of the heat spreader. If the penetration depth is defined as the distance from the base of the fin to the point where the temperature fluctuation is less than 0.1°C, then the penetration depth for the temperature profile shown in Fig. 15 is 6.1 mm. Illuminating the die area covers 1.0 cm², illuminating the die area and a sufficient edge area to prevent lateral conduction effects on the die area requires illumination of 4.9 cm².

Similarly, the penetration depth for a 40 Hz signal is 3.4 mm with overillumination covering 2.8 cm²; and at 100 Hz, the penetration depth is 2.1 mm with over-illumination covering 2.0 cm². Assuming the radiant intensity is uniform over the entire illuminated area, over-illumination requires 4.9 times more radiant power at 10 Hz, 2.1 times more at 40 Hz and 2.0 times the power at 100 Hz.

6 Conclusions

Time-leading temperature control in a distributed-parameter thermal system has been evaluated in one and two dimensions. A particular focus has been the testing of packaged, high-power, integrated circuits. The analysis identifies the control power required to bound the temperature variation of a system having time-dependent self-heating if control is by time-varying heat conduction to a position distant from the location being controlled.

The results may be very useful in the design of active thermal control systems for testing of electronic devices and for understanding the impact of electronic test-sequence designs and packaging design on the practical limits of temperature control. Three areas of operation for thermal control have been identified. At high frequencies, active control is not required because the temperature deviation without control is below the desired tolerance: steady (DC) cooling is all that is needed. At sufficiently low frequencies, thermal control can be obtained using a system's available control power. For intermediate frequencies, either control is not possible at the system's rated control power and desired temperature tolerance, or larger temperature deviations have to be accepted as a result of the system's limitation on control power.

This analysis can be applied to any situation where the temperature control source is separated from the active region where temperature control is desired, and should have value for systems other than electronics testing equipment.

Experimental tests of this analysis have been performed on prototype microprocessors, with good agreement [7]. These tests will be the subject of a future paper.

Nomenclature

$A(x)$ = cross-sectional area of IHS fin [m²]
A_0 = base cross-sectional area of IHS fin [m²]
A = mathematical constant, Eq. (10)
a_t = thermal diffusivity [m²/s]
B = mathematical constant, Eq. (11)
Bi_{ds} = Biot number for die-side of IHS, b/kR_t
Bi_{IHS} = Biot number for top side IHS, $h_c b/k$
b = integrated heat spreader thickness [m]
C, C_1, C_2 = mathematical constants
C_n = constant in infinite series
c_p = specific heat capacity at constant pressure [J/kg·K]
D, E, F = mathematical constants, Eq. (18) [W²/m⁴·K²]
G = mathematical constant, Eq. (23) [W²/m⁴·K²]
h_c = average convective transfer coefficient [W/m²·K]
i = the imaginary number, $\sqrt{-1}$
k = thermal conductivity [W/m·K]
L = fin length [m]
L = unsteady diffusion scale in IHS, $\sqrt{\omega/2a_t}$ [m⁻¹]
M = energy transfer correction factor, Eq. (39)
N = mathematical constant, Eq. (23) [W²/m⁴·K²]
m = mass of die per unit area [kg/m²]
P = mathematical constant, Eq. (24); or fin perimeter [m]
PS_1, PS_2 = mathematical constants, Eq. (32)
PS_3 = mathematical constant, Eq. (46)
Q_{sq} = square-wave die power density [W/m²]
Q_{tr} = triangular wave die power density [W/m²]
Q_d = die power density [W/m²]
Q_{da} = corrected die power density [W/m²], Eq. (43)

Q_c = control power density [W/m^2]
R = mathematical constant, Eq. (25)
R_t = thermal contact resistance [K·m^2/W]
S = ratio of die timescale to IHS diffusion timescale, Eq. (49)
T = fin temperature matrix [K]
T_{air} = air temperature [K]
T_{die} = die temperature [K]
T_{ref} = reference temperature—often taken as zero [K]
T_{BF} = IHS die-side temperature [K]
t = time [s]
U, V = mathematical constants, Eq. (28)
W = complex temperature solution
X = real part of complex temperature solution [K]
x = distance from reference face of integrated heat spreader [m]

Greek Symbols

α, β, γ = phase shifts [rad]
α = shaped fin geometry factor
α_n = infinite series constant
λ = lumped frequency response of die, $1/(mc_p R_t)$ [s^{-1}]
τ = imaginary part of complex temperature; or period of square/triangular wave [s]
θ = temperature defect, $(T - T_{ref})$ [K]
ω = frequency of die power variation [rad/s]

References

[1] Pfahnl, A. C., Lienhard V, J. H., and Slocum, A. H., 1999, "Thermal Management and Control in Testing Packaged Integrated Circuit Devices," *Proc. 34th Intersociety Energy Conversion Conf.*, Vancouver BC, Paper No. 1999-01-2723.

[2] Tadayon, P., 2000, "Thermal Challenges During Microprocessor Testing," Intel Technology Journal, **Q3**.

[3] Kromann, G. B., 1996, "Thermal Management of a C4/Ceramic-Ball-Grid Array: The Motorola Power PC 603 and PowerPC 604 RISC Microprocessors," *Proceedings of the Twelfth IEEE SEMI-THERM Symposium*, pp. 36–42.

[4] Malinoski, M., Maveety, J., Knostman, S., and Jones, T., 1998, "Test Site Thermal Control System for At-Speed Manufacturing Testing," *Proc. IEEE Intl. Test Conf.*, Washington, DC, pp. 119–128.

[5] Pfahnl, A. C., Lienhard V, J. H., and Slocum, A. H., 1998, "Temperature Control of a Handler Test Interface," *Proc. IEEE Intl. Test Conf.*, Washington, DC, pp. 114–118.

[6] Viswanath, R., Wakharkar, V., Watwe, A., and Lebonheur, V., 2000, "Thermal Performance Challenges From Silicon to Systems," Intel Technology Journal, **Q3**.

[7] Sweetland, M., 2001, "*Design of Thermal Control Systems for Testing of Electronics,*" Ph.D. thesis, Massachusetts Institute of Technology, Cambridge, MA.

[8] Tustantswkyj, J., and Babcock, J. B., 1998, "Temperature Control System for an Electronic Device Which Achieves a Quick Response by Interposing a Heater Between the Device and a Heat Sink," U.S. Patent #5,821,505.

[9] Tustaniwskyj, J. I., and Babcock, J. W., 1997, "Constant Temperature Control of a Device Under Test (DUT): Part 1, *Advances in Electronic Packaging,*" **2**, pp. 2031–2036.

[10] Carslaw, H. S., and Jaeger, J. C., 1959, *Conduction of Heat in Solids*, 2nd edition, Oxford University Press, Oxford.

[11] Mills, A. F., 1995, *Heat and Mass Transfer*, Irwin, Chicago, IL.

[12] Robertson, J. S., Bolinger, K., Glasser, L. M., Sloane, N. J. A., and Gross, R., *CRC Standard Mathematical Tables and Formulas*, Daniel Zwillinger, ed. CRC Press, Boca Raton, Chpt. 1.

[13] Aziz, A., and Kraus, A. D., 1995, "Transient Heat Transfer in Extended Surfaces," Appl. Mech. Rev., **48**(7), pp. 317–350.